Experimental Study on Surface Integrity of Single-Crystal Nickel-Based Superalloy Under Various Machining Processes

Srinivasa Rao Nandam, **A. Venugopal Rao**, **Amol A. Gokhale**, and **Suhas S. Joshi**

Abstract Nickel-based superalloys have the ability to retain superior mechanical and chemical properties at elevated temperatures. Therefore, these alloys become an ideal material choice for use in the hot sections of gas turbine engines. Advanced cast, single-crystal castings offer higher creep strength and thermal fatigue resistance than the columnar grained and polycrystalline castings. The castings undergo certain precision machining operations to obtain required fitment geometries during the engine assemblies. However, the nickel-based superalloys are considered as difficult-to-cut materials. High cutting forces and heat are generated while machining these alloys, which results in premature failure of cutting tools and poor integrity of the machined surfaces. The surface integrity aspects are of prime concern in the aerospace applications. This paper presents the results of the vital surface integrity aspects (i.e., surface topography and surface metallurgy) of a 2nd-generation single-crystal nickel-based superalloy under various precision machining process, namely milling, grinding WEDM and AWJM, which induces certain thermo-mechanical loads. It is observed that the ground surface has a highest surface finish (0.2 μm Ra) by the cutting and polishing action of multiple cutting points under higher cutting velocity. WEDM surface has lowest machining effect zone (10 μm) though it has highest surface roughness, misorientation angle, and degree of work hardening on the machined surface. Recrystallization and surface cracks were not observed at the machined surfaces under the subjected machining conditions.

Keywords Single-crystal nickel-based superalloy · Machining process · Surface integrity · Surface topography · Surface metallurgy

S. R. Nandam (✉) · A. Venugopal Rao
Defence Metallurgical Research Laboratory, DRDO, Hyderabad 500058, India
e-mail: srinivas-nandam.dmrl@gov.in

S. R. Nandam · A. A. Gokhale · S. S. Joshi
Department of Mechanical Engineering, IIT Bombay, Mumbai 400076, India
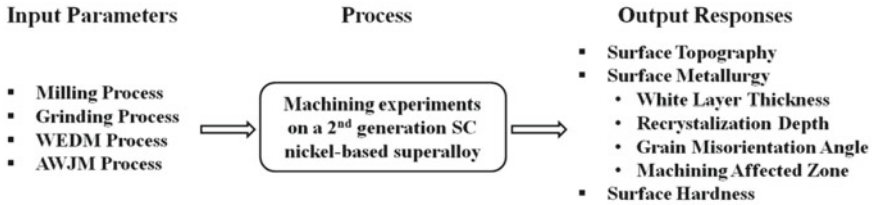
1   Introduction

Nickel-based superalloys have an exceptional combination of high-temperature strength, toughness, and resistance to degradation in corrosive and oxidizing environments. Therefore, these alloys become an ideal material choice for use in the hot sections of gas turbine engines for aerospace and power generation applications [1]. A noteworthy feature of nickel-base alloys is that they can be used for load-bearing applications at temperatures up to 80% of melting temperature (1000 °C) of the alloy [2].

The major phases present in nickel-based superalloys are γ and γ'. The continuous matrix, γ is a face-centered cubic (FCC) nickel-based austenitic phase that contains a high percentage of high strength and refractory elements. This matrix has high mechanical properties by the solid solution strengthening and high modulus. The primary strengthening phase, γ' is Ni_3(Al/Ti) coherently precipitating phase with an ordered L_{12} (FCC) crystal structure. Interestingly, the flow stress of the γ' increases with increasing temperature up to 650 °C due to Kear Wilsdorf lock [3]. In addition, γ' is quite ductile and thus imparts strength to the matrix without lowering the fracture toughness.

Nickel-based superalloys can be cast into components of complex shapes and/or internal configurations with metallurgically controlled uniform microstructure. Vacuum investment casting process is employed to produce cost-effective components with a high degree of dimensional accuracy, surface finish, and structural integrity [4]. Initially, the gas turbine blades were made as polycrystal (equi-axed) castings; later, development of the columnar-grained castings resulted in some significant improvements in creep strength and thermal fatigue resistance. Advanced cast, single-crystal (SC) nickel-based superalloy castings offer further improvement of high-temperature capabilities and resulting in superior turbine engine performance and durability [5]. The SC castings thus produced by the vacuum investment casting process undergo various machining operations to obtain fitment geometries for the engine assemblies. The nickel-based superalloys are considered as hard and difficult-to-cut materials due to high strength, hot hardness, fracture toughness and work hardening, and low thermal conductivity [6]. Higher cutting forces and heat are generated while machining these alloys, which result in premature failure of cutting tools and poor integrity of the machined surfaces [7].

The surface integrity (SI) of a machined component is the sum of all the elements that describe the conditions existing on or at the surface. The term was coined initially by Field and Kahles in the year 1964 [8]. The formation of a white layer at the machined surface is attributed to severe plastic deformation, grain refinement, phase transformation under rapid heating and quenching [9–12]. The SI aspects of the component are of prime concern in aerospace applications as the failures are primarily caused due to fatigue, creep, and stress corrosion, etc. [13].

Although there have been numerous studies on different aspects of cutting process over the years on superalloys, the properly published literature on SI aspects in the machining of SC nickel-based superalloys is not available. The SC superalloys

Input Parameters

- Milling Process
- Grinding Process
- WEDM Process
- AWJM Process

Process

Machining experiments on a 2nd generation SC nickel-based superalloy

Output Responses

- Surface Topography
- Surface Metallurgy
  - White Layer Thickness
  - Recrystalization Depth
  - Grain Misorientation Angle
  - Machining Affected Zone
- Surface Hardness

Fig. 1 Overall theme of the experimental investigation

are highly sensitive to thermo-mechanical loads. Hence, a systematic experimental study has been carried on a commercial second-generation single-crystal nickel-based superalloy, CMSX-4 superalloy by using various precision conventional and unconventional machining process, such as vertical milling, surface grinding, wire electric discharge machining (WEDM), and abrasives water jet machining (AWJM), respectively, which induces certain thermo-mechanical loads.

This paper focuses on the surface topography and surface metallurgy of the machined surfaces. The overall theme of the experimental study with input parameters and output responses is presented in Fig. 1.

2 Experimental Setup

2.1 Work Material

The single-crystals of the superalloy were supplied by Cannon Muskegon Corporation, USA, in the form of round rods with axis parallel to [001] direction. The nominal composition of CMSX-4 superalloy by weight percent is shown in Table 1.

This alloy maintains its ultra-high strength even at high temperatures by solid solution strengthening and precipitation hardening through the balanced alloy chemistry [14]. Rhenium element in this alloy mainly partitions into the γ matrix, which retards coarsening of γ' strengthening phase and increases γ/γ' misfit. Therefore, this alloy exhibits good resistance to excessive γ' growth during service. The physical and mechanical properties of CMSX-4 alloy from the supplier technical data are shown in Table 2.

**Table 1** Nominal chemical composition of CMSX-4 alloy in wt.%

Cr	Co	Mo	Ti	Al	W	C	Ta	Re	Hf	Ni
6.5	9.6	0.6	1.0	5.6	6.4	0.05	6.5	3.0	0.1	Balance

Table 2 Physical and
mechanical properties of
CMSX-4 alloy

Property	Unit	Value
Density @ RT	kg/m^3	8700
Thermal conductivity @ RT	W/m K	8
Melting temperature	°C	1380
0.2% proof yield strength @ 760 °C	MPa	980
Ultimate tensile strength @ 760 °C	MPa	1200
Elongation @ 760 °C	%	10
Reduction of area @ 760 °C	%	20

2.2 Specimen Preparation

Solid casting blocks were cut by a precision WEDM process from the fir tree side
of SC turbine blade castings, which were manufactured with <001> grain growth
direction from the prefix bottom seeding and directional solidification technique
through vacuum investment casting process. The test specimens were of length of
47 mm, width of 30 mm, and thickness of 12 mm. The micrographs of transverse to the
grain growth direction of the base metal in as-cast condition are shown in Fig. 2. The
optical micrographs reveal that the casting has four-fold dendrite core morphology
and eutectic phases in the inter-dendrite region. These eutectic phases can be seen
as bright lamellar regions in the inter-dendrite region. The high magnification SEM
images (Fig. 2b) of the dendritic core show the uniform distribution of γ' phase
embedded in the γ matrix.
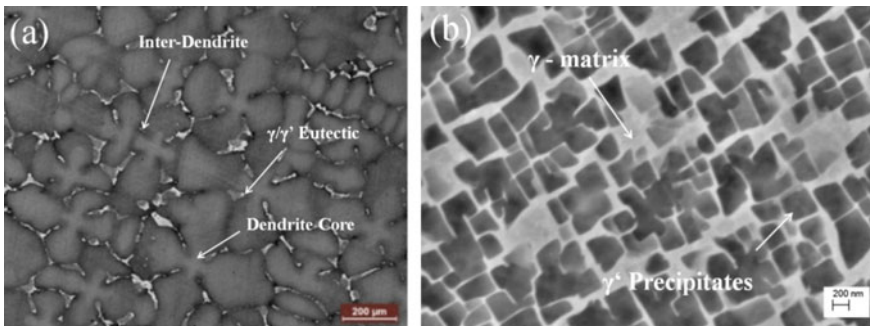
Fig. 2 Micrographs of transverse to the grain growth direction of the CMSX-4 alloy in as-cast
condition **a** Optical under 50× magnification and **b** SEM under 50,000× magnification

2.3 Machining Experiments

It is known that the milling and grinding process is conventional machining process, wherein the cutting action carries out by the combination of thermal and mechanical loads. The WEDM process is an unconventional machining process, wherein the cutting action carries out by the thermal erosion. The AWJM process is also an unconventional machining process, wherein the cutting action is carried out by the mechanical erosion from the high kinetic energy of water and abrasives. The thermo-mechanical loads in qualitative and specific energy in quantitative manner of the subjected machining process are shown in Fig. 3.

Milling Process: A knee-type conventional vertical milling machine (*FN2V model from M/s HMT, India*) of spindle motor power of 5.5 kW and rotational speed of 1800 per min was used. The sample was firmly fixed on the table, and face milling operations were performed with the solid carbide insert number TPN 2204 PDR 3040 (*M/s Sandvik Coromant, Pune*) fitted into a 100-mm-diameter cutter of 8 flutes. The flood coolant with a stable emulsion of 1:20 water ratio was employed with cutting speed of 50 m/min, table feed of 16 mm/min, and depth of cut of 0.2 mm.

Grinding Process: Grinding experiments were performed by a conventional horizontal spindle-type surface grinding machine (*PRAGA 452P model from M/s HMT, India*). The power rating of the spindle drive was 1.5 kW, and the maximum speed was 2800 rpm. A conventional tool room-type (white color) alumina-abrasive wheel of specification A60K5V8 (*M/s Carborundum Universal Limited, Chennai*) was used. The wheel has an outer diameter of 200 mm, inner diameter of 31.75 mm, and width of 20 mm. The table speed of 1.7 m/min, wheel speed of 1540 m/min, and depth of cut of 0.03 mm were used along with the soluble cutting oil, Servocut S grade with 3% concentration.

WEDM Process: The cutting experiments were conducted with 0.25-mm-diameter hard brass wire by a submerged-type precision WEDM machine (*CNC Ultracut S2 model from M/s Electronica Machine Tools, Pune*). Gap voltage of 36 V, current of
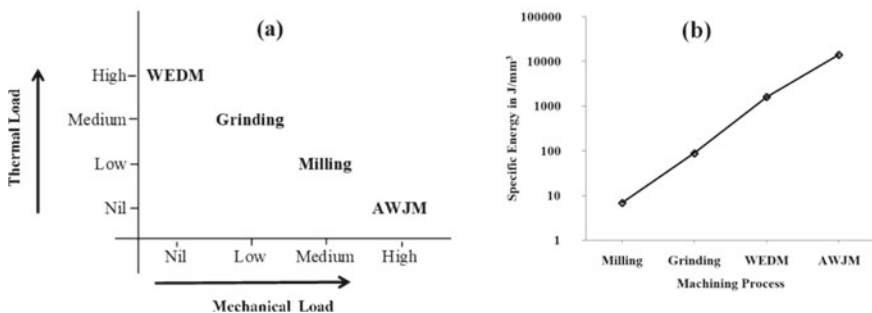
Fig. 3 Precision machining processes **a** thermo-mechanical loads and **b** semi-log plot of specific energies

1.4 A, time ON of 10 μs, cutting speed of 0.5 mm/min, and wire tension of 11 N were used along with the de-ionized water with total dissolved salts of below 3 ppm as dielectric.

A **WJM Process**: The cutting experiments were conducted with 80 mesh size garnet abrasives and 0.7 mm diameter sappier orifice nozzle by a water jet machining center (*55,100 model from M/s Omax, USA*). The parameters of surface quality of 5 number (i.e., high), water jet pressure of 255 MPa, abrasive flow rate of 340 g/min, traverse speed of 35 mm/min, and stand-off distance of 3 mm were used during the experiments.

2.4 Characterization Techniques

The surface roughness measurements were carried out on the machined surface by using a contact-type instrument (*Form Talysurf Intra model from M/s Taylor Hobson, UK*) with a 2 μm conisphere-shaped diamond stylus at 3 different locations along the machining direction. A cross-section of 12 mm $\times$ 12 mm with 10 mm thick was extracted from the machined surfaces of each machining process by using a precision WEDM. These geometries were mounted into the 1-inch size Bakelite molds and polished using a series of silicon carbide emery papers and diamond paste. The cleaned surfaces were etched by a commercial Kalling's 2 regent. The microstructural analysis was performed by an optical microscope (*DM 4000 M model from M/s Leica Microsystems GmbH, Germany*) and a scanning electron microscope (*EVO-18 SEM model from M/s Carl Zeiss, Germany*). The white-layer thickness was measured on the digital micrographs by using an image processing software (*Image J*). The recrystallization, crystal orientation, and mis-orientation angle studies were carried by using the electron backscatter diffraction (EBSD) technique (*Gemini SEM 300 model from Carl Zeiss GmbH, Germany*). The hardness on the machined surfaces was measured by using a micro-Vickers hardness instrument (*MMT XZ model from M/s Matsuzawa, Japan*) with diamond pyramid indenter under 0.5 kg load and dwell time of 10 s.

3 Results and Discussions

Optical images of the cross-section of the machined surfaces in Fig. 4 show that the machined surfaces have not consisted of micro-cracks.

The surface machined by WEDM has highest surface irregularities, and AWJM has the highest waviness.
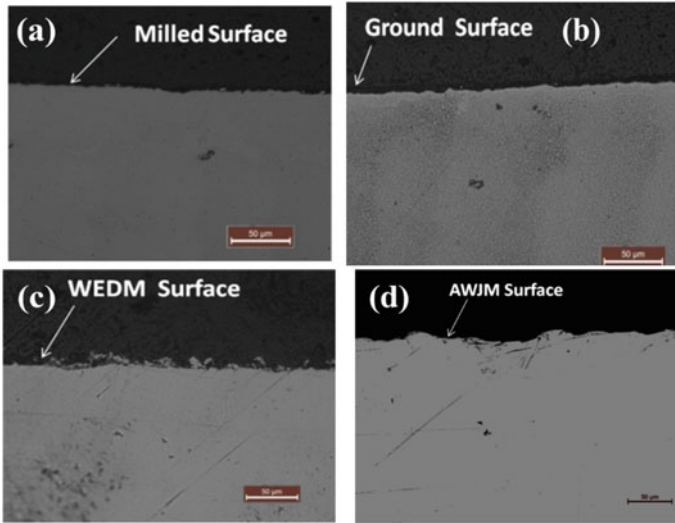
Fig. 4 Optical images (200X) of the machined surfaces of **a** milled, **b** ground, **c** WEDM and **d** AWJM process

3.1 Surface Roughness

The results of the average surface roughness are reported in Fig. 5. It is observed that the ground surface has the highest surface finish due to the cutting and polishing action of abrasives. The WEDM surface has the lowest surface finish due to higher surface irregularities by the discrete spark erosions and deposition of debris.

The milled surface has a better surface finish due to the engagement of multiple cutting inserts.
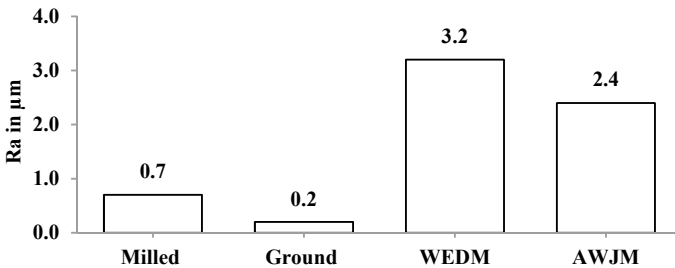
Fig. 5 Average surface roughness of the machined surfaces under subjected conditions
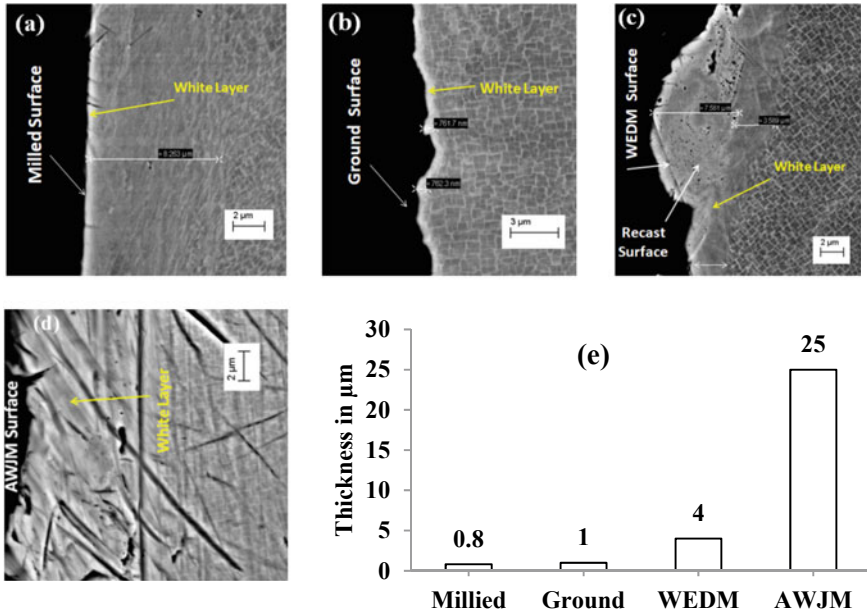
Fig. 6 SEM images (10,000×) of machined surfaces of **a** milled, **b** ground, **c** WEDM, **d** AWJM, and **e** results of white-layer thickness

3.2 White-Layer Thickness

The SEM images of the cross-section of the machined surfaces are shown in Fig. 6.

It can be seen that the machined surface by AWJM has the highest white-layer thickness due to higher mechanical loads while cutting, whereas the milled surface has the lowest value due to lower specific energy.

3.3 Recrystallization Depth

The results of the recrystallization studies on the machined surfaces by EBSD technique are shown in Fig. 7.

It is observed that none of the machining process could generate recrystallization defects under applied working conditions; however, a significant deformation (shown in red color at the location of 3rd column in the figure) was observed for the milling process due to multidirectional cutting forces.
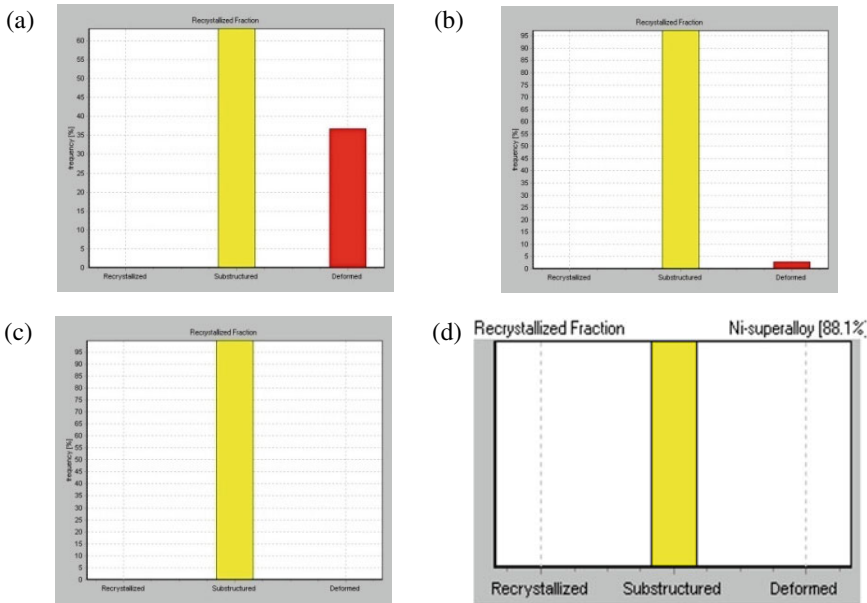
Fig. 7 Recrystallization results of **a** milled, **b** ground, **c** WEDM and **d** AWJM surfaces
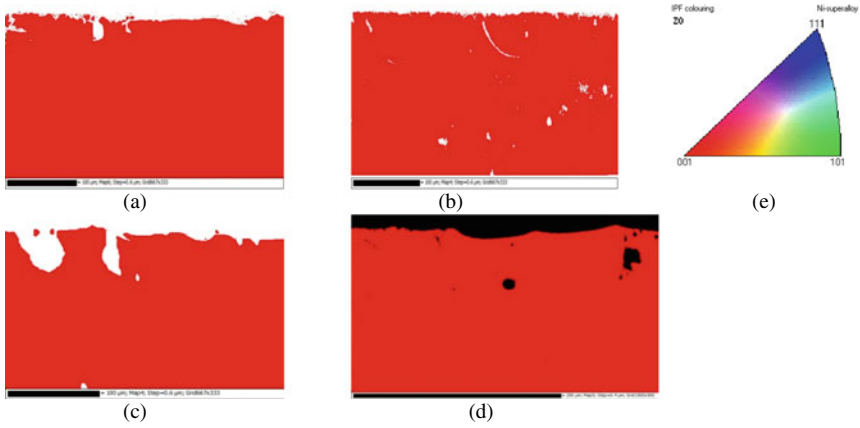
3.4 Crystal Orientation Direction

The machined surfaces were further analyzed by EBSD technique for crystal orientation mapping. The results along with inverse pole figure (IPF) color key are shown in Fig. 8.

It was observed that the machined surface has the crystal orientation equal to <001> direction; it was the same as that of the base metal casting.
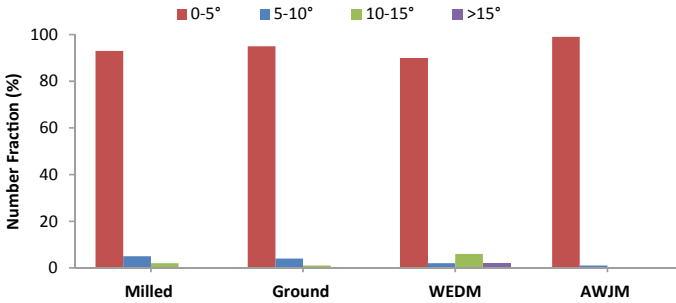
3.5 Misorientation Angle

The EBSD results of the distribution of grain boundary misorientation angles are shown in Fig. 9. It was observed that the surfaces under all machining process have a higher fraction of misorientation angle in the range from 0 to 5° only. AWJM surface has negligible distribution beyond 0 to 5° range, whereas the WEDM surface has a small number of misorientation angles beyond 5° and up to 15°.

The spread of WEDM surface could be due to the high temperature exposures by the discrete electric sparks. Formation of the crack-free surface was attributed to low misorientation angles.

Fig. 8 Crystal orientation results of **a** milled, **b** ground, **c** WEDM and **d** AWJM surfaces of CMSX-4 superalloy, and **e** IPF key


Fig. 9 Misorientation angles of the grain boundaries of milled, ground, WEDM and AWJM surfaces of CMSX-4 superalloy

3.6 Machining Affected Zone

The deformation images of the machined surface by EBSD technique are shown in Fig. 10. It can be seen that the milled surface has the highest deformation zone up to the maximum depth of 100 μm from the surface, whereas the WEDM has the lowest deformation depth of 10 μm.

The ground surface has the lower deformation depth than the milled surface. The ground surface images reveal the existence of slip lines below the machined surface. This could be due to localized thermo-mechanical loads.
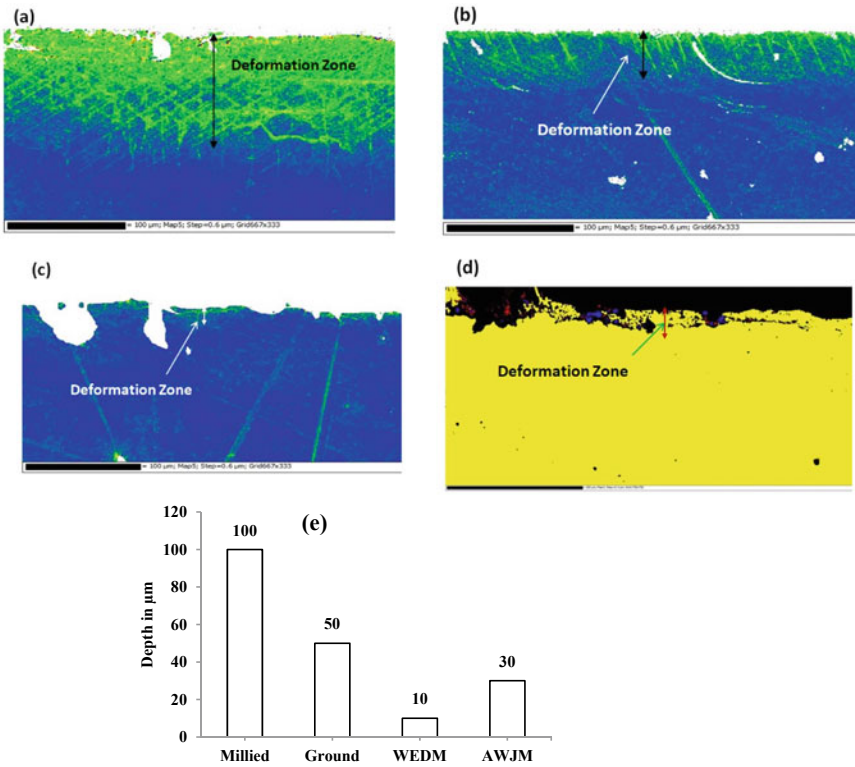
Fig. 10 Machining affected zone of CMSX-4 superalloy under **a** milling, **b** grinding, **c** WEDM and **d** AWJM process
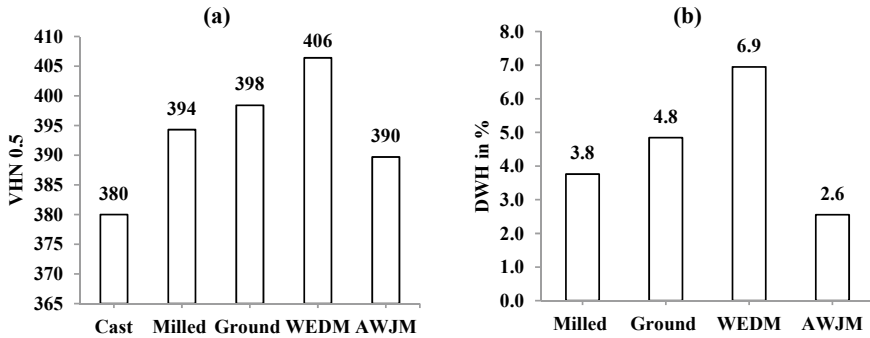
3.7 Surface Hardness

The average surface hardness values of the machined surfaces are shown in Fig. 11a.

The degree of surface hardening (DSH) in percentage was calculated by using the below equation:

$$DSH = \frac{(MSH - BSH)}{BSH} \times 100 \tag{1}$$

where **MSH** is the surface hardness of the machined surface and **BSH** is the surface hardness of the base metal in VHN. The results of DSH are shown in Fig. 11b. It can be seen that the machined surfaces have less than 10% DSH.

The WEDM has a higher DSH due to highest thermal loads during the cutting. The AWJM has a lower DSH though it has highest specific energy. This could be due to the direction of dominant cutting force in parallel to the machined surface.

Fig. 11 Surface hardness of the machined surfaces of CMSX-4 alloy under various machining process **a** average Vickers hardness and **b** DSH

4 Conclusions

Machining experiments were conducted on a 2nd-generation single-crystal nickel-based superalloy, CMSX-4 alloy in as-cast condition by milling, grinding, WEDM and AWJM process, which induces certain thermo-mechanical loads of various order. The following conclusions are drawn from the experimental study.

- The ground surface has achieved the best surface roughness of 0.2 μm Ra due to the cutting and polishing actions by the abrasives, whereas the WEDM surface has achieved the poor surface roughness of 3.2 μm Ra due to the deposition of discrete micro-debris on the machined surface. The machined surface of AWJM has highest waviness due to the divergence of the water jet.
- The specific energy is attributed to the formation of white-layer thickness. The AWJM surface has the highest value due to highest specific energy (mechanical load), and the milled surface has the lowest due to least specific energy.
- Though the milled process has lower specific energy, the milled surface has the highest machining affected zone with high plastic deformation depth due to the multidirectional action of cutting forces during cutting. The AWJM surface has the least amount of machining affected zone due to alignment of dominant cutting force in parallel direction to the machined surface.
- The thermal loads are attributed to the formation of misorientation angles. WEDM surface has a wide range of misorientation angles up to 15° by the high thermal loads, whereas AWJM has the least values of the angles.
- The thermal loads are also attributed to the hardening of the machined surfaces The WEDM surface has the highest amount of DSH due to the formation of a recast layer under rapid heating and cooling.
- Surface cracks, changes in the crystal orientation, and recrystallization were not observed on any of the machined surfaces under the machining conditions.

The chosen machining parameters, therefore, appear appropriate for machining the CMSX-4 superalloy, which obtained a higher integrity on the machined surfaces.

References

1. Pollock TM, Tin S (2006) Nickel based superalloys for advanced turbine engines: chemistry, microstructure, and properties. J Propuls Power 22(2):361–374
2. Reed RC (2006) The superalloys—fundamentals and applications. Cambridge University Press
3. Onyszko A, Kubiak K, Sieniawski J (2009) Turbine blades of the single crystal nickel based CMSX-6 superalloy. J Achiev Mater Manuf Eng 32(1):66–69
4. Spikesley GE (1979) Investment casting. Mater Eng Appl 1:328–334
5. Frasier DJ, Whetstone JR, Harris K, Erickson GL, Schwer RE (1990) Process and alloy optimization for CMSX-4 superalloy single crystal airfoils. In: Presented at COST 501/505 Conference, Belgium, pp 1281–1300
6. Arunachalam R, Mannan MA (2000) Machinability of nickle-based high temperature alloys. J Mach Sci Technol 4(1):127–168
7. Coelho RT, Silva LR, Braghini Jr A, Bezerra AA (2004) Some effects of cutting edge preparation and geometric modifications when turning Inconel 718 at high cutting speeds. J Mater Proces Technol 148(1):147–153
8. Bellows G, Tishler N (1970) Introduction to surface integrity, Pamplet 1, TM70-974, GE, Aircraft Engine Group, Cincinnati, USA
9. Arunachalam RM, Mannan MA, Spowage C (2004) Surface integrity when machining age hardened IN 718 with coated cutting tools. Int J Mach Tools Manuf 1481–1491
10. Saoubi RM, Outeiro JC, Chandrasekaran H, Dillon OW Jr, Jawahir IS (2008) A review of surface integrity in machining and its impact on functional performance and life of machined products. Int J Sustain Manuf 1(1/2):203–236
11. Pawade RS, Joshi SS, Brahmankar PK (2008) Effect of machining parameters and cutting edge geometry on surface integrity of high-speed turned IN718. Int J Mach Tools Manuf 48:15–28
12. Thakur A, Gangopadhyay S (2016) State-of-the-art in surface integrity in machining of nickel-based superalloys. Int J Mach Tools Manuf 100:25–54
13. Carter TJ (2005) Common failures in gas turbine blades. Eng Fail Anal 12:237–247
14. Harris K, Wahl JB (2004) Improved single crystal superalloys. CMSX-4 and CMSX-486 Superalloys 45–52